

# HUBBLE PARAMETER AND BARYON ACOUSTIC OSCILLATION MEASUREMENT CONSTRAINTS ON THE HUBBLE CONSTANT, THE DEVIATION FROM THE SPATIALLY FLAT $\Lambda$ CDM MODEL, THE DECELERATION-ACCELERATION TRANSITION REDSHIFT, AND SPATIAL CURVATURE

HAI YU,<sup>1,2,\*</sup> BHARAT RATRA,<sup>2,†</sup> AND FA-YIN WANG<sup>1,3,‡</sup>

<sup>1</sup>*School of Astronomy and Space Science, Nanjing University, Nanjing 210093, China*

<sup>2</sup>*Department of Physics, Kansas State University, 116 Cardwell Hall, Manhattan, KS 66506, USA*

<sup>3</sup>*Key Laboratory of Modern Astronomy and Astrophysics (Nanjing University), Ministry of Education, Nanjing 210093, China*

(Dated: March 13, 2018)

## ABSTRACT

We compile a complete collection of reliable Hubble parameter  $H(z)$  data to redshift  $z \leq 2.36$  and use them with the Gaussian Process method to determine continuous  $H(z)$  functions for various data subsets. From these continuous  $H(z)$ 's, summarizing across the data subsets considered, we find  $H_0 \sim 67 \pm 4$  km/s/Mpc, more consistent with the recent lower values determined using a variety of techniques. In most data subsets, we see a cosmological deceleration-acceleration transition at  $2\sigma$  significance, with the data subsets transition redshifts varying over  $0.33 < z_{\text{da}} < 1.0$  at  $1\sigma$  significance. We find that the flat- $\Lambda$ CDM model is consistent with the  $H(z)$  data to a  $z$  of 1.5 to 2.0, depending on data subset considered, with  $2\sigma$  deviations from flat- $\Lambda$ CDM above this redshift range. Using the continuous  $H(z)$  with baryon acoustic oscillation distance-redshift observations, we constrain the current spatial curvature density parameter to be  $\Omega_{K0} = -0.03 \pm 0.21$ , consistent with a flat universe, but the large error bar does not rule out small values of spatial curvature that are now under debate.

*Keywords:* cosmological parameters — large-scale structure of universe — cosmology: observations

\* yuhai@smail.nju.edu.cn

† ratra@phys.ksu.edu

‡ fayinwang@nju.edu.cn

## 1. INTRODUCTION

In the standard spatially flat  $\Lambda$ CDM cosmological model (Peebles 1984), the cosmological constant  $\Lambda$  dominates the current cosmological energy budget and powers the currently accelerating cosmological expansion. Cold dark matter (CDM) and baryonic matter are the second and third biggest contributors to the energy budget now, followed by small contributions from neutrinos and photons. Earlier on, non-relativistic (cold dark and baryonic) matter dominated and drove the decelerating cosmological expansion. For reviews of this scenario, see Ratra & Vogeley (2008); Martin (2012); Huterer & Shafer (2018). Many different observations are largely consistent with the standard picture, including cosmic microwave background (CMB) anisotropies (Planck Collaboration 2016), baryon acoustic oscillation (BAO) peak position data (Alam et al. 2017), Hubble parameter measurements (Farooq et al. 2017), and Type Ia supernovae observations (Betoule et al. 2014), but there is still room for some dark energy dynamics or spatial curvature, among other possibilities.

In this context, the Hubble parameter data, the cosmological expansion rate as a function of redshift  $z$ ,  $H(z)$ , is particularly interesting. Current  $H(z)$  data covers a large redshift range,  $0.07 \leq z \leq 2.36$  (Simon et al. 2005; Stern et al. 2010; Moresco et al. 2012; Blake et al. 2012; Font-Ribera et al. 2014; Delubac et al. 2015; Moresco 2015; Moresco et al. 2016; Alam et al. 2017), larger than that covered by the Type Ia supernovae. Not only can the  $H(z)$  data be used to constrain the usual cosmological parameters, such as the non-relativistic matter and dark energy density parameters (Samushia & Ratra 2006),<sup>1</sup> they can also be used to trace the cosmological deceleration-acceleration transition (Farooq & Ratra 2013; Jesus et al. 2017), and be used to measure the Hubble constant  $H_0$  (Busti et al. 2014; Chen et al. 2017; Wang & Meng 2017). And in conjunction with distance-redshift data,  $H(z)$  measurements can be used to constrain spatial curvature (Clarkson et al. 2007, 2008).

In this paper, we build on and extend these results. We first gather together a complete collection of currently available  $H(z)$  data, which does not include older results from earlier analyses of data subsets nor estimates that are no longer believed to be reliable. Some of these measurements are correlated, so we account for these correlations when using the Gaussian Process (GP) method to determine a continuous  $H(z)$  function that best approximates the discrete  $H(z)$  measurements we have collected. As far as we are aware, such correlations have been ignored in all previous GP method  $H(z)$  determinations. (The technique we have developed here for accounting for such correlations will be useful for future analyses.) From the GP method-determined  $H(z)$  we measure  $H_0$  and find it is more consistent with other lower  $H_0$  estimates (Chen & Ratra 2011a), but the high local measurement (Riess et al. 2016) lies within the  $2\sigma$  range of our estimates here.

For the first time, we use the evolution of  $\Omega_{m0}$  with redshift (derived from continuous  $H(z)$  functions determined by applying the GP method to the observed  $H(z)$  data) to test the spatially flat  $\Lambda$ CDM model, finding agreement up to a  $z$  of 1.5 or 2, depending on which combination of discrete  $H(z)$  data we use to determine the GP method continuous  $H(z)$ . Above a redshift of 1.5 or 2, there are  $2\sigma$  indications of deviation from flat- $\Lambda$ CDM, but it has only recently become possible to measure  $H(z)$ 's at or above  $z = 2$  so it is perhaps best to wait for better and more higher- $z$  data before forming a strong opinion about these deviations.

We also use these  $H(z)$ 's to study the cosmological deceleration-acceleration transition and measure the redshift of this transition,  $z_{\text{da}}$ . Our results here qualitatively agree with those found earlier, with the GP method  $H(z)$  constraints on  $z_{\text{da}}$  being significantly weaker than those determined by using cosmological model templates (Farooq et al. 2017).

When the open inflation (Gott 1982; Ratra & Peebles 1994, 1995) and closed inflation (Hawking 1984; Ratra 1985, 2017) model energy density inhomogeneity power spectra are used to analyze the Planck 2015 CMB anisotropy data (Planck Collaboration 2016), they favor a closed universe with current spatial curvature density parameter magnitude of a percent or two (Ooba et al. 2017a,b,c; Park & Ratra 2018). It is important to measure spatial curvature in as many other ways as possible so as to definitely establish whether the universe is spatially flat or spatially curved. The GP method-determined continuous  $H(z)$  can be used, in conjunction with BAO measured distance as function of redshift, to constrain the current value of the spatial curvature energy density parameter  $\Omega_{K0}$  (Clarkson et al. 2007, 2008). Here, we generalize the method proposed by Yu & Wang (2016) for measuring  $\Omega_{K0}$ , by now also accounting — for the first time — for the correlations between some of the BAO distance measurements. (The technique we have developed here for accounting for such correlations will be useful for future analyses.) We find that the data are

<sup>1</sup> Early developments include Samushia et al. (2007); Chen & Ratra (2011b); Farooq et al. (2013a) while more recent work may be traced back through Tripathi et al. (2017); Lonappan et al. (2017); Rezaei et al. (2017); Magana et al. (2017); Anagnostopoulos & Basilakos (2017); Martins (2017).

consistent with a flat universe, with  $\Omega_{K0}$  error bars of about 0.2, much too large to test the findings of Ooba et al. (2017a,b,c), and Park & Ratra (2018).

Our paper is organized as follows. In the next section, we introduce our  $H(z)$  data compilation and discuss how we organize these data into 12 different samples. In Sec. 3, we use the GP method to compute continuous  $H(z)$  functions that best represent our 12 samples of discrete  $H(z)$  data. In this section, we also measure  $H_0$  from each of these samples. In Sec. 4, we use the continuous  $H(z)$  functions to test whether the current  $H(z)$  data are consistent with the flat- $\Lambda$ CDM model or not, and in Sec. 5, we measure the cosmological deceleration-acceleration transition redshift  $z_{\text{da}}$  for each sample. In Sec. 6, we gather the best available BAO measurements and use them in a joint analysis with one of the continuous  $H(z)$ 's to constrain  $\Omega_{K0}$ . We conclude in Sec. 7.

## 2. HUBBLE PARAMETER DATA

The Hubble parameter measurements we use are taken from Table 1 of Farooq et al. (2017) with the following alterations. We now also include the recent redshift  $z = 0.4$  cosmic chronometric measurement (Ratsimbazafy et al. 2017). We drop the three Blake et al. (2012) WiggleZ radial BAO points — because of the partial overlap of the WiggleZ and BOSS spatial regions (Beutler et al. 2016) that is difficult to account for in our analyses — choosing to instead retain the more precise BOSS radial BAO measurements (Alam et al. 2017). We rescale the five BAO  $H(z)$  measurements in our compilation to a fiducial sound horizon length  $r_{d,\text{fid}} = 147.60 \pm 0.43$  Mpc determined from the TT + lowP + lensing Planck 2015 analysis (Planck Collaboration 2016). This results in 36  $H(z)$  measurements that are tabulated in Table 1. This is a complete collection of currently available, reliable  $H(z)$  data.

Of these 36  $H(z)$  measurements, 31 are determined using the cosmic chronometric technique<sup>2</sup>, three correlated measurements are from the radial BAO signal in the galaxy distribution, and the last two at  $z = 2.34$  and  $2.36$  are measured from the BAO signal in the Ly $\alpha$  forest distribution alone or cross-correlated with QSOs. The covariance matrix of the three galaxy distribution radial BAO  $H(z)$  measurements is (Alam et al. 2017)

$$\begin{pmatrix} 3.65 & 1.78 & 0.93 \\ 1.78 & 3.65 & 2.20 \\ 0.93 & 2.20 & 4.45 \end{pmatrix} \quad (1)$$

and is accounted for in our computations here.

In addition, we also consider two different values for  $H_0$ ,  $68.0 \pm 2.8$  km/s/Mpc (Chen & Ratra 2011a) and  $73.24 \pm 1.74$  km/s/Mpc (Riess et al. 2016), to study the effect of the assumed  $H_0$  value on our results.

Given that BAO results depend on the assumed cosmological model used to analyze the BAO data (this is likely to be a small effect since there is fairly strong evidence that the true cosmological model cannot be very different from the models assumed for these analyses), it is useful to examine a variety of different combinations of the  $H(z)$  data.

Our Sample 1.0 comprises the 31 cosmic chronometric measurements and the two highest redshift Ly $\alpha$  measurements, with labels a and c in column 3 of Table 1, for a total of 33 points. Sample 2.0 is the full collection of 36 measurements in Table 1. Sample 3.0 consists of only the 31 cosmic chronometric measurements which are labeled a in column 3 of Table 1. Sample 4.0 adds to these the three Alam et al. (2017) BAO measurements, labeled b in column 3 of Table 1, for a total of 34 points.

We add  $H_0 = 68.0 \pm 2.8$  km/s/Mpc as the prior value of the Hubble constant to the samples above and denote this new set as Samples 1\_1, 2\_1, 3\_1, and 4\_1, with 34, 37, 32, and 35 data points respectively. In order to study the effect of the choice of the prior  $H_0$  value, we also consider Samples 1\_2, 2\_2, 3\_2, and 4\_2 which instead use  $H_0 = 73.24 \pm 1.74$  km/s/Mpc as the prior value. All in all, we consider 12 different  $H(z)$  samples.

## 3. SMOOTHED $H(Z)$ FUNCTION FROM THE GAUSSIAN PROCESS METHOD

To leverage the  $H(z)$  data, it is necessary to assume a cosmological model that is characterized in terms of a small number of free parameters and to use the  $H(z)$  data to constrain these free parameters.  $\Lambda$ CDM (Peebles 1984) and  $\phi$ CDM (Peebles & Ratra 1988; Ratra & Peebles 1988) are two physically consistent dark energy (either  $\Lambda$  or a dynamical scalar field  $\phi$ ) CDM models that have been used for this purpose. Often, a parameterization, XCDM, in

<sup>2</sup> As discussed in Moresco et al. (2016), see their Table 3 for example, cosmic chronometric  $H(z)$  error bars are dominated by systematic uncertainty.

**Table 1.** Hubble parameter data.

$z$	$H(z)$ [km/s/Mpc]	Method	Reference
0.07	$69 \pm 19.6$	a	(1)
0.09	$69 \pm 12$	a	(2)
0.12	$68.6 \pm 26.2$	a	(1)
0.17	$83 \pm 8$	a	(2)
0.179	$75 \pm 4$	a	(3)
0.199	$75 \pm 5$	a	(3)
0.2	$72.9 \pm 29.6$	a	(1)
0.27	$77 \pm 14$	a	(2)
0.28	$88.8 \pm 36.6$	a	(1)
0.352	$83 \pm 14$	a	(3)
0.38	$81.9 \pm 1.9$	b	(4)
0.3802	$83 \pm 13.5$	a	(5)
0.4	$95 \pm 17$	a	(2)
0.4004	$77 \pm 10.2$	a	(5)
0.4247	$87.1 \pm 11.2$	a	(5)
0.4497	$92.8 \pm 12.9$	a	(5)
0.47	$89 \pm 50$	a	(6)
0.4783	$80.9 \pm 9$	a	(5)
0.48	$97 \pm 62$	a	(6)
0.51	$90.8 \pm 1.9$	b	(4)
0.593	$104 \pm 13$	a	(3)
0.61	$97.8 \pm 2.1$	b	(4)
0.68	$92 \pm 8$	a	(3)
0.781	$105 \pm 12$	a	(3)
0.875	$125 \pm 17$	a	(3)
0.88	$90 \pm 40$	a	(6)
0.9	$117 \pm 23$	a	(2)
1.037	$154 \pm 20$	a	(3)
1.3	$168 \pm 17$	a	(2)
1.363	$160 \pm 33.6$	a	(8)
1.43	$177 \pm 18$	a	(2)
1.53	$140 \pm 14$	a	(2)
1.75	$202 \pm 40$	a	(2)
1.965	$186.5 \pm 50.4$	a	(8)
2.34	$223 \pm 7$	c	(9)
2.36	$227 \pm 8$	c	(10)

Notes: a. Cosmic chronometric method. b. BAO signal in galaxy distribution. c. BAO signal in Ly $\alpha$  forest distribution alone, or cross-correlated with QSOs. Reference: (1). Zhang et al. (2014), (2). Simon et al. (2005), (3). Moresco et al. (2012), (4). Alam et al. (2017), (5). Moresco et al. (2016), (6). Ratsimbazafy et al. (2017), (7). Stern et al. (2010), (8). Moresco (2015), (9). Delubac et al. (2015), (10). Font-Ribera et al. (2014).

which dynamical dark energy is modeled as an ideal fluid, has also been used, but this parameterization is physically inconsistent and does not adequately approximate the dark energy evolution of  $\phi$ CDM (Podariu & Ratra 2001).

Here, we use the GP method to determine a continuous function  $H(z)$  that best represents the discrete Hubble parameter data we have compiled in Table 1.<sup>3</sup> The GP method was first used cosmologically by Holsclaw et al. (2010a,b, 2011); Shafieloo et al. (2012); Seikel et al. (2012a,b). From a continuous  $H(z)$ , we are able to extract interesting cosmological information, including the values of  $H_0$  and  $z_{\text{da}}$ .

### 3.1. Gaussian Process method

The GP method is used to obtain a continuous function  $f(x)$  that is best representative of a discrete set of measurements  $f(x_i) \pm \sigma_i$  at  $x_i$ , where  $i = 1, 2, \dots, N$  and  $\sigma_i$  are the  $1\sigma$  error bars. The GP method assumes that the value of the function at any position  $x$  is a random variable that follows a gaussian distribution. And the expectation and standard deviation of this gaussian distribution,  $\mu(x)$  and  $\sigma(x)$ , are determined from the discrete data through a defined covariance function (or kernel function)  $k(x, x_i)$  and are given by

$$\mu(x) = \sum_{i,j=1}^N k(x, x_i)(M^{-1})_{ij}f(x_j), \quad (2)$$

and

$$\sigma(x) = k(x, x) - \sum_{i,j=1}^N k(x, x_i)(M^{-1})_{ij}k(x_j, x), \quad (3)$$

where the matrix  $M_{ij} = k(x_i, x_j) + c_{ij}$  and  $c_{ij}$  is the covariance matrix of the observed data, given by eqn. (1) for the correlated measurements and otherwise diagonal with elements  $\sigma_i^2$ . Equations (2) and (3) specify the posterior distribution of the extrapolated points.

Given eqns. (2) and (3), the continuous function  $f(x)$  can be determined once we have a suitable covariance function  $k(x, x')$ . In practice, there are many possible covariance functions. Here, we consider three covariance functions to illustrate the ‘‘model dependence’’ of our results. The usual covariance function, and that used in most of our analyses here, is the gaussian

$$k(x, x') = \sigma_f^2 \exp\left[-\frac{(x - x')^2}{2l^2}\right]. \quad (4)$$

Here,  $\sigma_f$  and  $l$  are parameters that control the strength of the correlation of the function value and the coherence length of the correlation in  $x$ , respectively. The other two covariance functions we use to examine the ‘‘model dependence’’ of our results are the Matérn and Cauchy ones. The forms of these are

$$k(x, x') = \sigma_f^2 \left[1 + \frac{\sqrt{3}|x - x'|}{l}\right] \exp\left[-\frac{\sqrt{3}|x - x'|}{l}\right], \quad (5)$$

and

$$k(x, x') = \sigma_f^2 \frac{l}{(x - x')^2 + l^2}. \quad (6)$$

(We find good consistency between the continuous functions we derive using the three different covariance functions.) The parameters  $\sigma_f$  and  $l$  are optimized for the observed data,  $f(x_i) \pm \sigma_i$ , by minimizing the log marginal likelihood function (Seikel et al. 2012a)

$$\ln \mathcal{L} = -\frac{1}{2} \sum_{i,j=1}^N [f(x_i) - \mu(x_i)](M^{-1})_{ij}[f(x_j) - \mu(x_j)] - \frac{1}{2} \ln |M| - \frac{1}{2} N \ln 2\pi, \quad (7)$$

where  $|M|$  is the determinant of  $M_{ij}$ .

In this work, we use the open-source Python package GaPP (Seikel et al. 2012a), which is widely used in cosmological studies (Seikel et al. 2012b; Bilicki & Seikel 2012; Cai et al. 2016; Wang et al. 2017a; Yu & Wang 2017). It can output

<sup>3</sup> Other methods have also been used to determine continuous functions that best represent discrete cosmological data (Mignone & Bartelmann 2008; Maturi & Mignone 2009; Benitez-Herrera et al. 2012; Montiel et al. 2014; Vitenti & Penna-Lima 2015; Semiz & Çamlıbel 2015).

the continuous function  $f(x)$  as well as its first derivative  $f'(x)$  once certain data and parameters are input. The derivative is computed from the smooth reconstructed function and its uncertainty is estimated from the covariance function. For detailed information about the Gaussian Process method and the package GaPP, see [Seikel et al. \(2012a\)](#) and [www.acgc.uct.ac.za/~seikel/GAPP/Documentation/Documentation.html](http://www.acgc.uct.ac.za/~seikel/GAPP/Documentation/Documentation.html).

### 3.2. Smoothed $H(z)$ function and $H_0$

In this section, we use the 12 samples of Sec. 2 and the GP method<sup>4</sup> summarized in the previous sub-section to compute continuous Hubble parameter functions  $H(z)$  and use them to constrain the value of the Hubble constant  $H_0$ .<sup>5</sup> The smoothed  $H(z)$  functions from all 12 samples are plotted in Figure 1. The three panels of the first column are the results from Samples 1\_0, 1\_1, and 1\_2, respectively and the other three columns are similar but for Sample 2, 3, and 4, respectively. From these  $H(z)$ , we can measure  $H_0$ ; these are listed in Table 2.

Table 2 also lists  $H_0$  values derived under the Matérn and Cauchy covariance function assumptions, in addition to those derived using the gaussian covariance function (which is used to compute the  $H(z)$  functions shown in Figure 1). We also plot all of the  $H_0$  values together (see the left panel of Figure 4). It is reassuring that changing the covariance function used does not significantly alter the estimated  $H_0$ , even more so when we use an  $H_0$  measurement in the determination of  $H(z)$ .

Comparing the three panels in each column in Figure 1, or the equivalent determined  $H_0$  values listed in Table 2, we see that if one of the  $H_0$  measurements is used in the determination of the continuous  $H(z)$ , then the resulting errors on the determined  $H_0$  are smaller. This is because the  $H_0$  measurements have much tighter error bars than the rest of the  $H(z)$  data we use.

The first row of Figure 1, or the corresponding  $H_0$  values listed in Table 2, show that all four of the non- $H_0$  samples we examine (Samples 1\_0, 2\_0, 3\_0, and 4\_0) favor a lower value of  $H_0$ , but with fairly large error bars (about  $\pm 4$  km/s/Mpc). These are consistent with the most recent median statistics estimate  $H_0 = 68 \pm 2.8$  km/s/Mpc ([Chen & Ratra 2011a](#)), which is consistent with earlier median statistics estimates ([Gott et al. 2001](#); [Chen et al. 2003](#)). These values are also quite consistent with cosmological-model-based determinations of  $H_0$  from  $H(z)$  data ([Chen et al. 2017](#)). Many recent estimates of  $H_0$  are also quite consistent with the median statistics measurement ([Calabrese et al. 2012](#); [Sievers et al. 2013](#); [Aubourg et al. 2015](#); [Semiz & Çamlıbel 2015](#); [Planck Collaboration 2016](#); [L’Huillier & Shafieloo 2017](#); [Luković et al. 2016](#); [Wang et al. 2017b](#); [Lin & Ishak 2017](#); [Abbott et al. 2017](#)). Of course, the error bars on  $H_0$  estimated here and in [Chen et al. \(2017\)](#) are large and the high local measurement of  $H_0 = 73.24 \pm 1.74$  km/s/Mpc ([Riess et al. 2016](#)) lies within the  $2\sigma$  confidence limits of our measurements here. In addition, we note that some other local expansion rate measurements find a slightly lower  $H_0$  with larger error bars ([Rigault et al. 2015](#); [Zhang et al. 2017](#); [Dhawan et al. 2018](#); [Fernández Arenas et al. 2017](#)).

## 4. TESTING THE FLAT- $\Lambda$ CDM MODEL

In the spatially flat  $\Lambda$ CDM model, which provides a reasonable description of the universe, the expansion history is  $H(z) = H_0 \sqrt{\Omega_{m0}(1+z)^3 + \Omega_{r0}(1+z)^4 + 1 - \Omega_{m0} - \Omega_{r0}}$  where  $\Omega_{m0}$  and  $\Omega_{r0}$  are the current values of the non-relativistic and relativistic matter density parameters. Solving, we have

$$\frac{[H^2/H_0^2 - 1]}{\Omega_{m0}[(1+z)^3 - 1]} = 1 - \frac{\Omega_{r0}[(1+z)^4 - 1]}{\Omega_{m0}[(1+z)^3 - 1]} \approx 1, \quad (8)$$

where  $\frac{\Omega_{r0}[(1+z)^4 - 1]}{\Omega_{m0}[(1+z)^3 - 1]} \sim 10^{-3}$  at  $z = 2$  and can be omitted because it is much smaller than 1 in the redshift range we care about and the uncertainties of  $H(z)$  data are relatively large. Therefore, we have

$$\Omega_{m0} = \left[ \left( \frac{H(z)}{H_0} \right)^2 - 1 \right] / [(1+z)^3 - 1], \quad (9)$$

which is a redshift-independent constant if flat- $\Lambda$ CDM is the correct description of the universe and so can be used to test the model ([Sahni et al. 2008](#)). To test whether this is constant, we compute the first derivative of the right hand

<sup>4</sup> We note that lower  $z$  parts of earlier compilations of  $H(z)$  data have been shown to not be inconsistent with Gaussianity and so probably consistent with the GP method requirement of Gaussianity ([Farooq et al. 2013b, 2017](#)).

<sup>5</sup> For earlier studies based on smaller  $H(z)$  compilations, see [Busti et al. \(2014\)](#); [Wang & Meng \(2017\)](#).

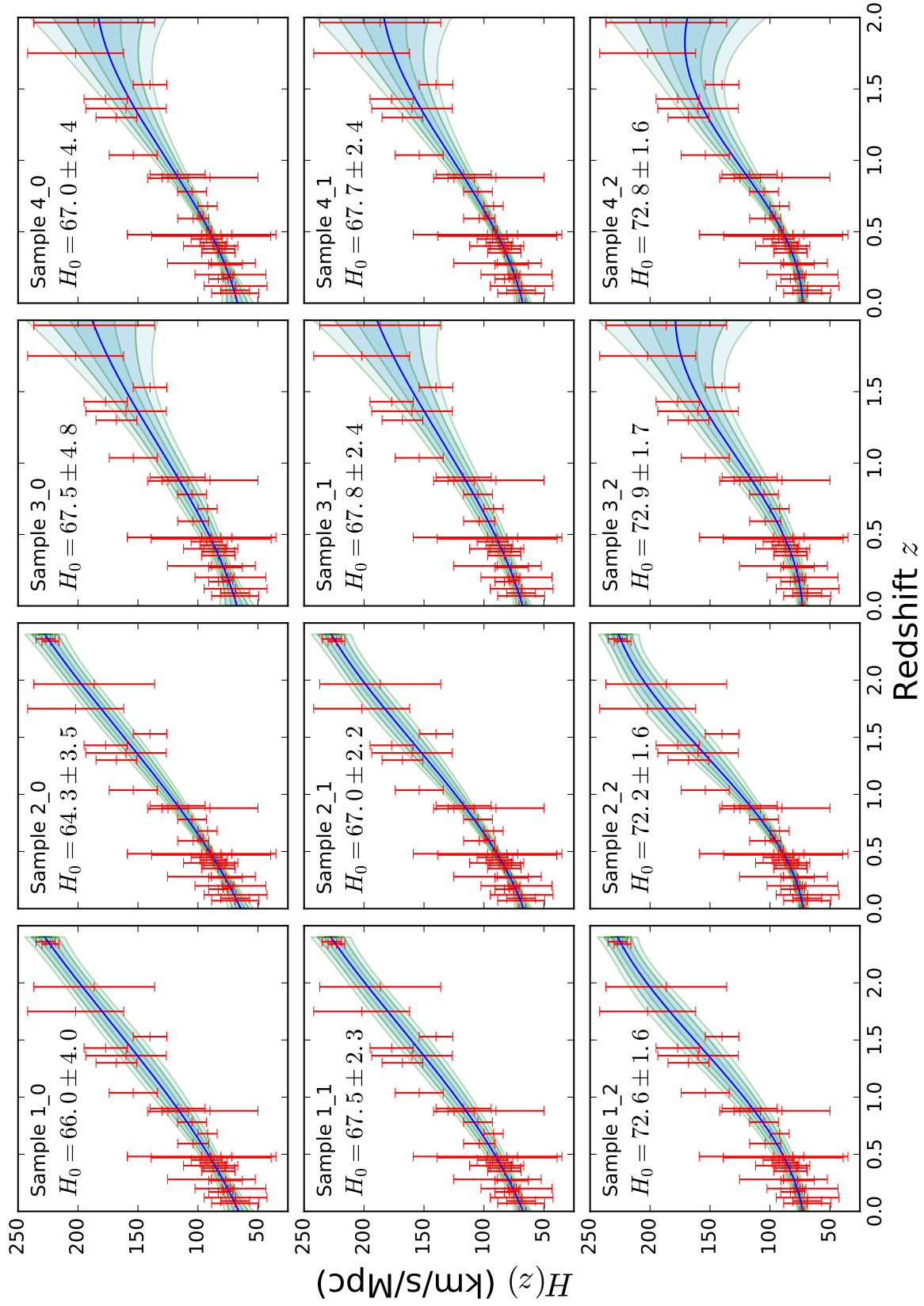


**Figure 1.** Smoothed  $H(z)$  functions for all 12 samples. The blue lines are the mean curves and the shadow areas are  $1\sigma$ ,  $2\sigma$ , and  $3\sigma$  confidence regions.

**Table 2.** Constraints on  $H_0$  and  $z_{\text{da}}$  from 12 samples and 3 different covariance functions.

Sample ID	Covariance Function	$H_0$ (km/s/Mpc)	$z_{\text{da}}$
Sample 1.0	G	$66.0 \pm 4.0$	$0.59^{+0.19}_{-0.32}$
	M	$67.8 \pm 5.3$	$0.57^{+0.27}_{-0.23}$
	C	$66.9 \pm 4.2$	$0.59^{+0.18}_{-0.24}$
Sample 1.1	G	$67.5 \pm 2.3$	$0.63^{+0.14}_{-0.14}$
	M	$67.9 \pm 2.5$	$0.57^{+0.26}_{-0.19}$
	C	$67.7 \pm 2.3$	$0.61^{+0.16}_{-0.13}$
Sample 1.2	G	$72.6 \pm 1.6$	$0.65^{+0.11}_{-0.08}$
	M	$72.8 \pm 1.7$	$0.57^{+0.22}_{-0.15}$
	C	$72.7 \pm 1.6$	$0.63^{+0.12}_{-0.09}$
Sample 2.0	G	$64.3 \pm 3.5$	$0.50^{+0.17}_{-0.25}$
	M	$66.4 \pm 4.8$	$0.46^{+0.32}_{-0.12}$
	C	$65.0 \pm 3.7$	$0.51^{+0.16}_{-0.21}$
Sample 2.1	G	$67.0 \pm 2.2$	$0.55^{+0.12}_{-0.10}$
	M	$67.6 \pm 2.4$	$0.47^{+0.31}_{-0.10}$
	C	$67.1 \pm 2.3$	$0.55^{+0.12}_{-0.10}$
Sample 2.2	G	$72.2 \pm 1.6$	$0.58^{+0.09}_{-0.07}$
	M	$72.7 \pm 1.7$	$0.46^{+0.34}_{-0.08}$
	C	$72.3 \pm 1.6$	$0.56^{+0.09}_{-0.07}$
Sample 3.0	G	$67.5 \pm 4.8$	$0.56^{+0.22}_{-0.25}$
	M	$68.8 \pm 6.3$	$0.55^{+0.23}_{-0.20}$
	C	$69.6 \pm 5.2$	$0.53^{+0.16}_{-0.14}$
Sample 3.1	G	$67.8 \pm 2.4$	$0.58^{+0.23}_{-0.13}$
	M	$68.1 \pm 2.5$	$0.55^{+0.45}_{-0.19}$
	C	$68.1 \pm 2.4$	$0.55^{+0.20}_{-0.12}$
Sample 3.2	G	$72.9 \pm 1.7$	$0.55^{+0.12}_{-0.08}$
	M	$72.9 \pm 1.7$	$0.54^{+0.21}_{-0.16}$
	C	$73.0 \pm 1.7$	$0.53^{+0.12}_{-0.08}$
Sample 4.0	G	$67.0 \pm 4.4$	$0.47^{+0.12}_{-0.13}$
	M	$67.7 \pm 5.5$	$0.44^{+0.56}_{-0.11}$
	C	$68.1 \pm 4.7$	$0.47^{+0.11}_{-0.10}$
Sample 4.1	G	$67.7 \pm 2.4$	$0.48^{+0.11}_{-0.08}$
	M	$67.9 \pm 2.5$	$0.45^{+0.55}_{-0.10}$
	C	$67.9 \pm 2.4$	$0.47^{+0.11}_{-0.08}$
Sample 4.2	G	$72.8 \pm 1.6$	$0.48^{+0.08}_{-0.05}$
	M	$72.8 \pm 1.7$	$0.44^{+0.56}_{-0.08}$
	C	$72.8 \pm 1.6$	$0.48^{+0.08}_{-0.05}$

Notes: G: Gaussian covariance function, M: Matérn covariance function, C: Cauchy covariance function.



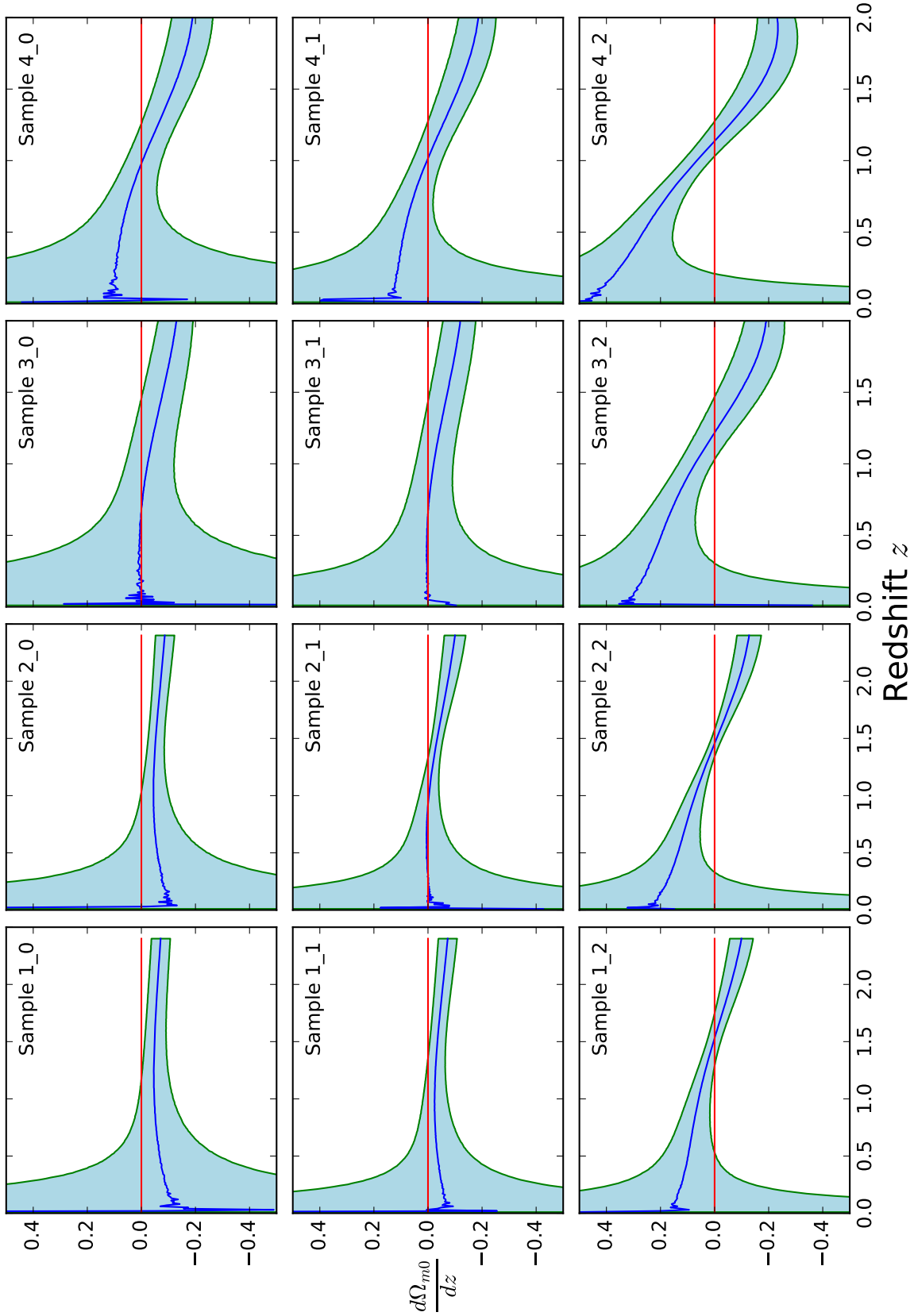


**Figure 2.**  $\frac{d\Omega_{m0}}{dz}$  of all the 12 samples. The blue lines are the mean curves and the gray areas are  $1\sigma$ ,  $2\sigma$ , and  $3\sigma$  confidence regions respectively. The red lines indicate  $\frac{d\Omega_{m0}}{dz} = 0$ .

side of this equation, which we label  $\frac{d\Omega_{m0}}{dz}$ . If this is significantly biased away from 0, it implies that  $\Omega_{m0}$  does evolve with redshift and that the data don't favor the flat- $\Lambda$ CDM model.<sup>6</sup>

The  $\frac{d\Omega_{m0}}{dz}$  function can be derived from the smoothed  $H(z)$  function and results for all 12 samples are shown in Figure 2. The  $H(z)$  data are largely consistent with the flat- $\Lambda$ CDM model, with some deviations at higher  $z$  for some of the samples. At  $2\sigma$ , in column 3 of Figure 2, for the 31 cosmic chronometric measurements alone or in combination with an  $H_0$  measurement, we see no deviation from flat- $\Lambda$ CDM except in the lowest panel above a  $z$  of about 1.9. Adding in the three Alam et al. (2017) radial BAO measurements, column 4 of Figure 2, we see deviation from flat- $\Lambda$  above about a redshift of 1.8 in the top and middle (with the added  $H_0 = 68 \pm 2.8$  km/s/Mpc point) panels, and above about a  $z$  of 1.6 in the lowest panel (with the added  $H_0 = 73.24 \pm 1.74$  km/s/Mpc point). Instead, when we consider the 31 cosmic chronometric measurements with the two highest  $z$  Ly $\alpha$  ones, column 1 of Figure 2, the trend is in the opposite direction, with the data being consistent with flat- $\Lambda$ CDM below a redshift of 1.9 or 2 for the top and middle panels, while in the lowest panel flat- $\Lambda$ CDM is adequate up to about a  $z$  of 2.2. The full  $H(z)$  data, in column 2, has a similar trend, with flat- $\Lambda$ CDM doing a reasonable job to a  $z$  of about 1.6 in the top two panels and to about 1.8 in the bottom panel.

So, depending on the sample considered, flat- $\Lambda$ CDM provides an adequate model to a redshift of 1.5 or 2, which is consistent with former a study (Lonappan et al. 2017). Higher  $z$   $H(z)$  data is inconsistent with flat- $\Lambda$ CDM at  $2\sigma$ . However, given that it has only recently become possible to make such high  $z$  measurements, it is probably best not to make too much of this disagreement. This is an interesting test and we look forward to soon learning more about whether or not flat- $\Lambda$ CDM provides an adequate description of the  $z \sim 2$  and higher universe, when better quality and more  $H(z)$  data becomes available.

## 5. CONSTRAINING THE COSMOLOGICAL DECELERATION-ACCELERATION TRANSITION REDSHIFT

In the standard cosmological picture, dark energy dominates the current cosmological energy budget and is responsible for the currently accelerating cosmological expansion; at earlier times non-relativistic — baryonic and cold dark — matter dominated the energy budget and powered the decelerating expansion. Farooq & Ratra (2013) used  $H(z)$  data to study this transition and measure the redshift of the transition,  $z_{\text{da}}$ , in a variety of cosmological models. For more recent similar analyses of compilations of  $H(z)$  measurements, see Capozziello et al. (2014); Moresco et al. (2016); Farooq et al. (2017). Here, we use the GP method  $H(z)$  continuous functions we have derived from the most up-to-date compilation of  $H(z)$  data to measure  $z_{\text{da}}$ .

The Friedmann equation is

$$\ddot{a}(z) = \frac{H^2}{1+z} - H \frac{dH}{dz}, \quad (10)$$

where  $a$  is the scale factor of the universe.  $z_{\text{da}}$  is the solution of  $\ddot{a}(z_{\text{da}}) = 0$ . Using the continuous  $H(z)$  functions obtained in Sec. 3.2 and eqn. (10), we can derive  $\ddot{a}(z)$  for each of the 12 samples and then solve for  $z_{\text{da}}$  from  $\ddot{a}(z_{\text{da}}) = 0$ .

Figure 3 shows the  $\ddot{a}(z)$  functions for the 12 samples, derived using the gaussian covariance function. From the functions plotted in the figure, we can read the values of  $z_{\text{da}}$ , which occur where the (central) blue and red lines cross (at lower  $z$ ). Similarly, the crossing points of the red line and the  $1\sigma$  confidence region boundary determine the  $1\sigma$  errors on  $z_{\text{da}}$ . The last column of Table 2 lists the lowest  $z_{\text{da}}$  value that solves the corresponding  $\ddot{a}(z_{\text{da}}) = 0$  for the 12 samples for each of the three covariance functions we use. We also plot all of the  $z_{\text{da}}$  values on a same figure for easy comparison (see the right panel of Figure 4). All of the determined values are largely consistent with each other no matter which sample or covariance function is used. From the listed  $z_{\text{da}}$  and the figure, we see that, depending on sample, there is a clear detection of a deceleration-acceleration transition in the  $1\sigma$  redshift range  $0.33 < z_{\text{da}} < 1.0$ . This is quite a broad range, with most of the larger  $z_{\text{da}}$   $1\sigma$  upper values coming from the Matérn covariance function case. This range is significantly larger than those determined by using cosmological models (Farooq & Ratra 2013; Capozziello et al. 2014; Semiz & Çamlıbel 2015; Moresco et al. 2016; Farooq et al. 2017) or a two-part piece-wise linear fit to the  $H(z)$  data (Moresco et al. 2016). This is probably because the GP method has more freedom than the cosmological model templates or the two-part piece-wise linear template. While, for a given covariance function, the GP method has only two parameters,  $\sigma_f$  and  $l$ , there is the additional freedom of being allowed to alter the covariance function assumed, thus resulting in a larger range for  $z_{\text{da}}$ . It is likely, given the present quality of the  $H(z)$  data,

<sup>6</sup> For an application of this test based on supernovae data, see Yahya et al. (2014).

**Table 3.** BAO distance measurements used in this work.

Variable	Redshift	Original Value (Mpc)	Rescaled Value (Mpc)	References
$D_V$	0.106	$456 \pm 27$	$456 \pm 27$	Beutler et al. (2011)
$D_V$	0.15	$(664 \pm 25)r_d/r_{d,\text{fid}}$	$659 \pm 25$	Ross et al. (2015)
$D_M$	0.38	$(1518 \pm 22)r_d/r_{d,\text{fid}}$	$1516 \pm 22$	Alam et al. (2017)
	0.51	$(1977 \pm 27)r_d/r_{d,\text{fid}}$	$1975 \pm 27$	
	0.61	$(2283 \pm 32)r_d/r_{d,\text{fid}}$	$2280 \pm 32$	
$D_V$	1.52	$(3843 \pm 147)r_d/r_{d,\text{fid}}$	$3838 \pm 147$	Ata et al. (2018)
$D_M$	2.33	$(37.77 \pm 2.13)r_d$	$5575 \pm 314$	Bautista et al. (2017)

that the cosmological model templates result in a more reliable determination of  $z_{\text{da}}$  than that obtained from the GP method here.

While there is some evidence in Figure 3 to suggest an early (additional) epoch of accelerated cosmological expansion, at  $2\sigma$  confidence, this is only in the lowest panel of column 4, for Sample 4.2, above a redshift of about 1.9, for the 31 cosmic chronometric and three Alam et al. (2017) BAO measurements and including  $H_0 = 73.24 \pm 1.74$  km/s/Mpc. More and better higher- $z$   $H(z)$  data will be needed to resolve this issue.

In the top row of Figure 3, we see that at  $2\sigma$  only Sample 4.0, 31 cosmic chronometric and three Alam et al. (2017) BAO measurements, shows evidence for low- $z$  acceleration and intermediate- $z$  deceleration, while Samples 1.0 and 2.0 show evidence only for intermediate- $z$  deceleration with Sample 3.0 consistent with  $\ddot{a}(z) = 0$  at  $2\sigma$ .

When an  $H_0$  measurement is included with the other  $H(z)$  data, in rows 2 and 3 of Figure 3, we see  $2\sigma$  evidence for low- $z$  acceleration and intermediate- $z$  deceleration in all panels, except in Sample 3.1 for the 31 cosmic chronometric measurements where there is no  $2\sigma$  evidence for intermediate- $z$  deceleration.

All in all, the results of the  $\ddot{a}(z_{\text{da}}) = 0$  analyses here are qualitatively consistent with those found earlier (Farooq & Ratra 2013; Capozziello et al. 2014; Moresco et al. 2016; Farooq et al. 2017). More and better  $H(z)$  data will allow the GP method to provide  $z_{\text{da}}$  estimates that can also be quantitatively compared to those derived from cosmological model templates.

## 6. CONSTRAINING SPATIAL CURVATURE

The GP method-determined  $H(z)$ , the cosmological expansion rate as a function of redshift, may be used in conjunction with BAO observations, which give a distance as a function of redshift, to measure spatial curvature (Clarkson et al. 2007, 2008; Mörtzell & Jönsson 2011; Sapone et al. 2014; Li et al. 2014; Takada & Doré 2015; Cai et al. 2016; Yu & Wang 2016; L’Huillier & Shafieloo 2017; Li et al. 2016; Wei & Wu 2017; Rana et al. 2017; Wang et al. 2017b). Here, we extend the test proposed by Yu & Wang (2016) to constrain spatial curvature, to now allow for correlations between the BAO measured distances. This method measures the spatial curvature density parameter  $\Omega_{K0}$  by using the relation between the co-moving radial and angular diameter distances

$$\frac{H_0 D_M(z)}{c} \sqrt{-\Omega_{K0}} = \sin \left( \frac{H_0 D_C(z)}{c} \sqrt{-\Omega_{K0}} \right). \quad (11)$$

Here,  $D_C(z) = \int_0^z \frac{cdz}{H(z)}$  is the co-moving radial distance,  $D_M(z) = (1+z)D_A(z)$  is the co-moving angular diameter distance,  $c$  is the speed of light,  $D_A(z)$  is the angular diameter distance, and for the open case with positive  $\Omega_{K0}$ , the  $\sin(x)$  is replaced with  $\sin(ix) = i \sinh(x)$ . We shall also have need for the angle-averaged distance  $D_V(z) = [czD_M^2(z)/H(z)]^{1/3}$ .

In Table 3 we compile BAO distance measurements we use. We rescale these to the baryon drag epoch fiducial sound horizon length  $r_{d,\text{fid}} = 147.60 \pm 0.43$  Mpc from the Planck 2015 TT + lowP + lensing analysis (Planck Collaboration 2016).

From Table 3, the vector of observed data is  $V_{\text{obs}} \equiv [D_V(0.106), D_V(0.15), D_M(0.38), D_M(0.51), D_M(0.61), D_V(1.52), D_M(2.33)]$ . In addition, with eqn. (11) and the smoothed  $H(z)$  function, we can construct the corresponding “model

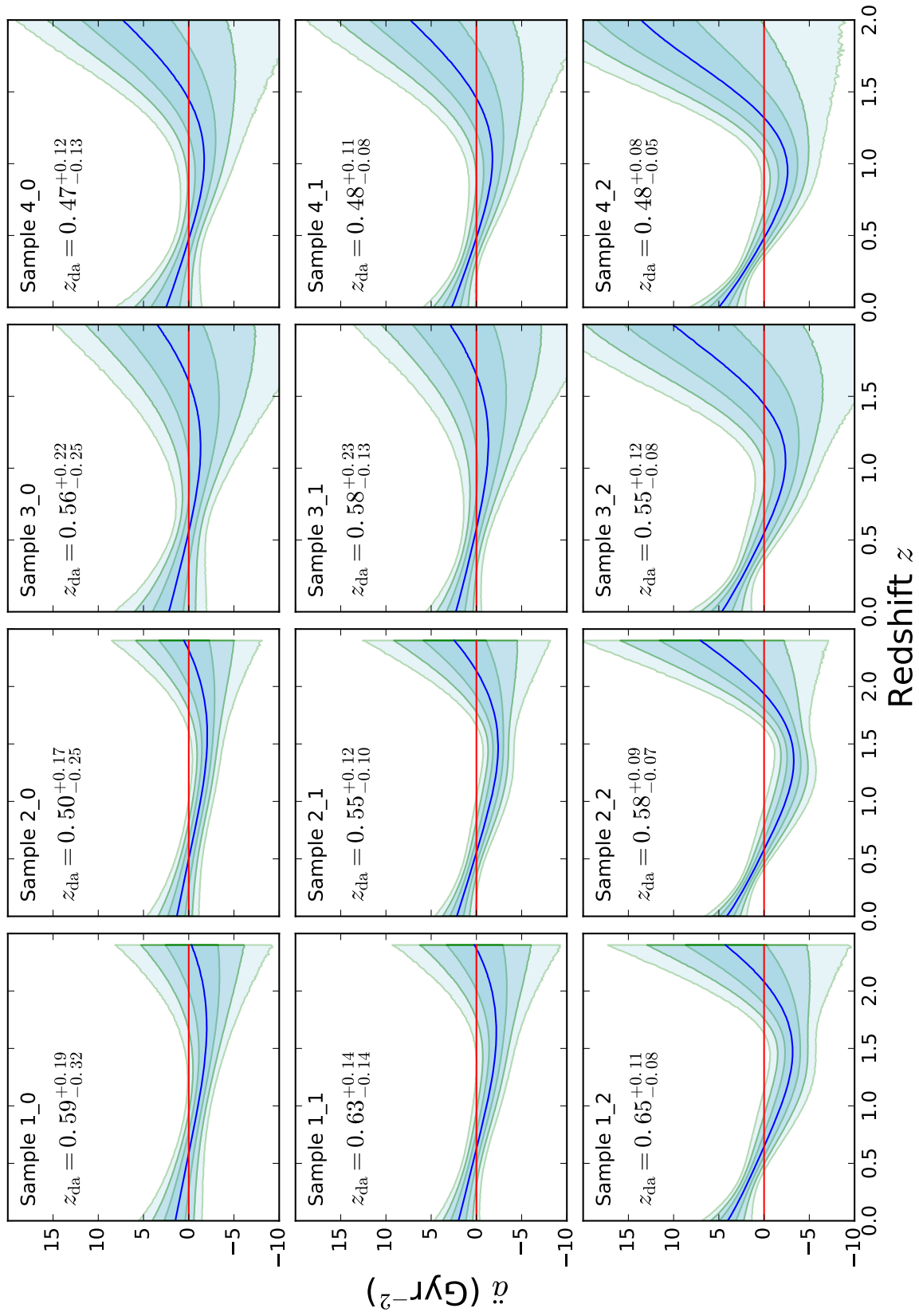


**Figure 3.**  $\ddot{a}(z)$  for the 12 samples. The blue lines are the mean curves and the gray areas are 1 $\sigma$ , 2 $\sigma$ , and 3 $\sigma$  confidence regions, respectively. The red lines indicate  $\ddot{a} = 0$ .

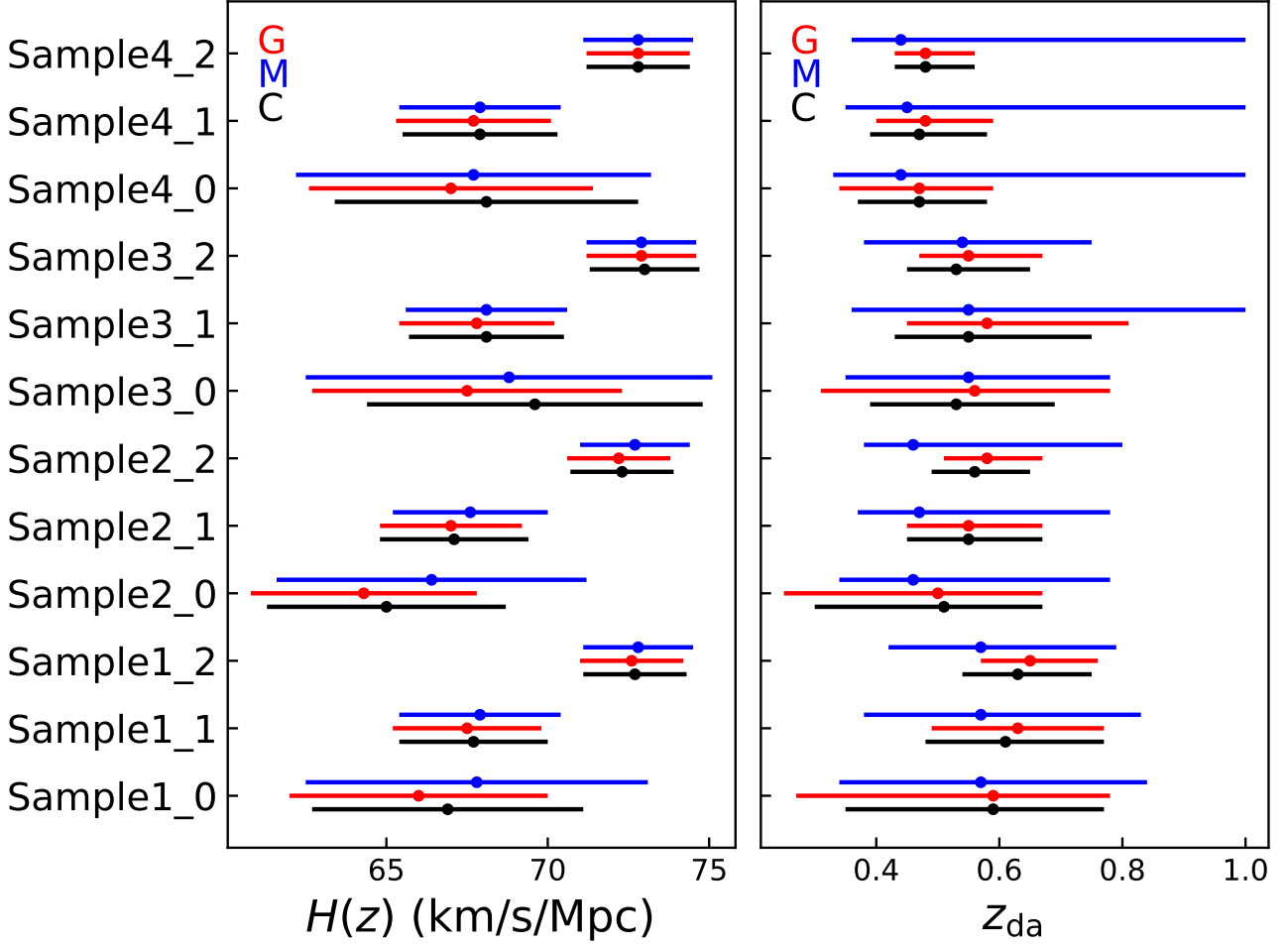


**Figure 4.** Determined  $H_0$  and  $z_{da}$  values for all 12 samples and three covariance functions. The errors are  $1\sigma$  confidence level. The red, blue, and black colors represent the gaussian, Matérn, and Cauchy covariance function determinations.

prediction” vector  $V_{th}(H_0, \Omega_{K0})$  which depends on the values of  $H_0$  and  $\Omega_{K0}$ . Here, we use the smoothed  $H(z)$  function derived from Sample 1\_0 to be able to make use of the BAO distance measurement at  $z = 2.33$ . (Sample 1\_0 is comprised of the 31 cosmic chronometric  $H(z)$  measurements as well as the two highest  $z$  BAO Ly $\alpha$  ones.) The two-dimensional log likelihood function is then given by

$$\ln[\mathcal{L}(\Omega_{K0}, H_0)] = -0.5(V_{obs} - V_{th})C^{-1}(V_{obs} - V_{th})^T, \quad (12)$$

where the covariance matrix of the observed BAO distances is

$$C = \begin{pmatrix} 729 & 0 & 0 & 0 & 0 & 0 & 0 \\ 0 & 616 & 0 & 0 & 0 & 0 & 0 \\ 0 & 0 & 483 & 294 & 140 & 0 & 0 \\ 0 & 0 & 294 & 727 & 441 & 0 & 0 \\ 0 & 0 & 140 & 440 & 1022 & 0 & 0 \\ 0 & 0 & 0 & 0 & 0 & 21556 & 0 \\ 0 & 0 & 0 & 0 & 0 & 0 & 98840 \end{pmatrix}. \quad (13)$$

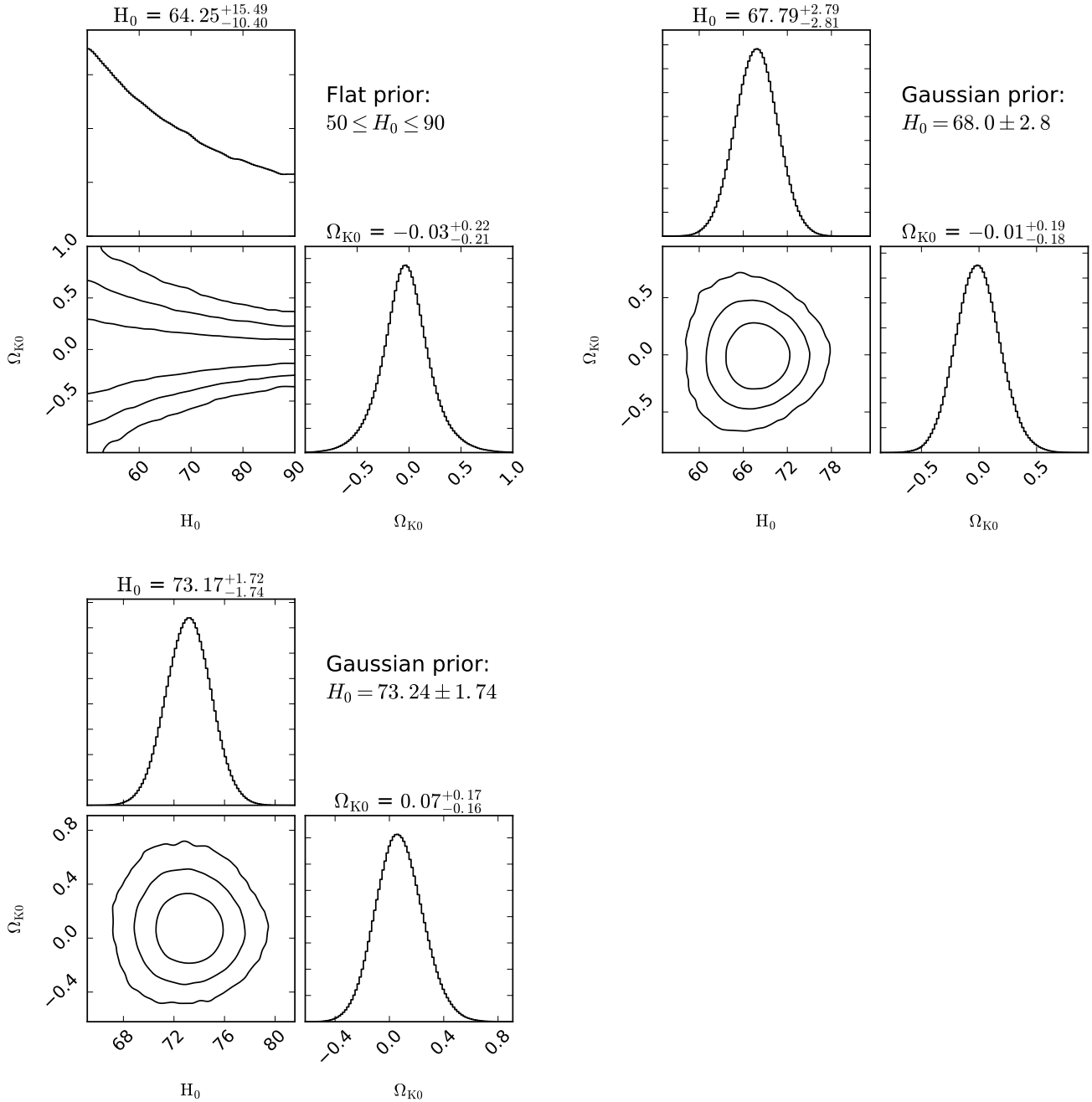


**Figure 5.** Constraints on  $\Omega_{K0}$  for the three different  $H_0$  priors. The left top panels present the flat prior non-zero over only  $50 \text{ km/s/Mpc} \leq H_0 \leq 90 \text{ km/s/Mpc}$ , the right top panels present results for the gaussian prior corresponding to  $H_0 = 68 \pm 2.8 \text{ km/s/Mpc}$ , while the last one is for the gaussian prior with  $H_0 = 73.24 \pm 1.74 \text{ km/s/Mpc}$ .

We use the open-source Markov chain Monte Carlo Python package *emcee* (Foreman-Mackey et al. 2013) for our analyses. The two-dimensional likelihood function depends on  $\Omega_{K0}$  and  $H_0$ . To derive one-dimensional  $H_0$  and  $\Omega_{K0}$  likelihoods and limits we need to assume priors. We use three priors for  $H_0$ , a flat prior, non-zero over 50–90 km/s/Mpc, and two gaussian priors with  $H_0 = 68.0 \pm 2.8 \text{ km/s/Mpc}$  (Chen & Ratra 2011a) and  $H_0 = 73.24 \pm 1.74 \text{ km/s/Mpc}$  (Riess et al. 2016). The  $\Omega_{K0}$  prior is chosen to be flat and non-zero over  $-1 \leq \Omega_{K0} \leq 1$ . Results are shown in Figure 5 for the gaussian covariance function case; the other two covariance functions lead to very similar results.

From Figure 5, we see that  $\Omega_{K0}$  is constrained to  $-0.03 \pm 0.21$ ,  $-0.01 \pm 0.19$ , and  $0.07 \pm 0.17$  when using the flat prior non-zero over the  $H_0$  range  $50 - 90$  km/s/Mpc, and the two gaussian priors with  $H_0 = 68 \pm 2.8$  km/s/Mpc and  $H_0 = 73.24 \pm 1.74$  km/s/Mpc respectively. These results are consistent with the results of earlier work that use  $H(z)$ , BAO, and other non CMB anisotropy data to measure  $\Omega_{K0}$  (Farooq et al. 2015; Yu & Wang 2016; Farooq et al. 2017; Li et al. 2016; Wei & Wu 2017; Xia et al. 2017; Rana et al. 2017; Wang et al. 2017a; Mitra et al. 2017). Although these results are mostly consistent with a flat universe, the uncertainties are large and more precise measurements of  $H(z)$  and the angular diameter distance at higher redshift are needed for tighter constraints on  $\Omega_{K0}$  and to check the findings of Ooba et al. (2017a,b,c), and Park & Ratra (2018).

## 7. CONCLUSION

We compile a complete collection of currently available, reliable  $H(z)$  data. Of these 36  $H(z)$  data points, 31 are measured by the cosmic chronometric technique, while 5 come from BAO observations. We use this compilation with the GP method to determine a continuous  $H(z)$  function, from which we measure  $H_0$ ,  $z_{\text{da}}$ , and  $\Omega_{K0}$  (in combination with BAO distance-redshift data) and use to test the flat- $\Lambda$ CDM model. While there has been a lot of earlier work on these issues, we have for the first time accounted for all known correlations between data points that have previously been ignored. We have also organized our  $H(z)$  data into 12 different samples to check for potential effects caused by the measurement or data reduction technique used or by the value assumed for  $H_0$ .

Averaging across the samples we use, we find  $H_0 \sim 67 \pm 4$  km/s/Mpc, more consistent with the recent lower values determined using a variety of techniques.

In most samples we consider, we see a cosmological deceleration-acceleration transition at  $2\sigma$  significance, with the data sample transition redshifts varying over  $0.33 < z_{\text{da}} < 1.0$  at  $1\sigma$  significance. This is significantly broader than the  $z_{\text{da}}$  range determined using cosmological model templates. The reason for this disagreement might be that the GP method allows a less steep expansion history at  $z > 1$ , than do the cosmological model templates, which make the  $\ddot{a}$  function flatter. This needs to be studied more carefully when more precise  $H(z)$  measurements become available.

We find that the flat- $\Lambda$ CDM model is consistent with the  $H(z)$  data to a  $z$  of 1.5 to 2.0 depending on the sample considered, with  $2\sigma$  deviations from flat- $\Lambda$ CDM above this redshift range. This also needs to be more carefully examined with future higher-quality  $H(z)$  data.

Using the continuous  $H(z)$  with BAO distance-redshift observations, a representative constraint on the current spatial curvature density parameter is  $\Omega_{K0} = -0.03 \pm 0.21$ . This is consistent with a flat universe, but the large error bar does not rule out small values of spatial curvature that might be of interest (Ooba et al. 2017a,b). Higher quality measurements of  $H(z)$  and  $D_M(z)$  at higher redshift are necessary to tighten this constraint, and these are likely to become available soon.

## 8. ACKNOWLEDGMENTS

This work is supported by the National Basic Research Program of China (973 Program, grant No. 2014CB845800), the National Natural Science Foundation of China (grants 11422325 and 11373022), the Excellent Youth Foundation of Jiangsu Province (BK20140016), and by DOE grant DE-SC0011840. Yu, H. also thanks the support of China Scholarship Council for studying abroad.

## REFERENCES

- Abbott, T. M. C., Abdalla, F. B., Annis, J., et al. 2017, arXiv:1711.00403
- Alam, S., Ata, M., Bailey, S., et al. 2017, MNRAS, 470, 2617 [arXiv:1607.03155]
- Anagnostopoulos, F., & Basilakos, S. 2017, arXiv:1709.02356
- Ata, M., Baumgarten, F., Bautista, J., et al. 2018, MNRAS, 473, 4773 [arXiv:1705.06373]
- Aubourg, E., Bailey, S., Bautista, J. E., et al. 2015, PhRvD, 92, 123516 [arXiv:1411.1074]
- Bautista, J. E., Busca, N. G., Guy, J., et al. 2017, A&A, 603, A12 [arXiv:1702.00176]
- Benitez-Herrera, S., Röpke, F., Hillebrandt, W., et al. 2012, MNRAS, 419, 513 [arXiv:1109.0873]
- Betoule, M., Kessler, R., Guy, J., et al. 2014, A&A, 568, A22 [arXiv:1401.4064]
- Beutler, F., Blake, C., Colless, M., et al. 2011, MNRAS, 416, 3017 [arXiv:1106.3366]
- Beutler, F., Blake, C., Koda, J., et al. 2016, MNRAS, 455, 3230 [arXiv:1506.03900]

- Bilicki, M., & Seikel, M. 2012, *MNRAS*, 425, 1664 [arXiv:1206.5130]
- Blake, C., Brough, S., Colless, M., et al. 2012, *MNRAS*, 425, 405 [arXiv:1204.3674]
- Busti, V. C., Clarkson, C., & Seikel, M. 2014, *MNRAS*, 441, L11 [arXiv:1402.5429]
- Cai, R.-G., Guo, Z.-K., & Yang, T. 2016, *PhRvD*, 93, 043517 [arXiv:1509.06283]
- Calabrese, E., Archidiacono, M., Melchiorri, A., & Ratra, B. 2012, *PhRvD*, 86, 043520 [arXiv:1205.6753]
- Capozziello, S., Farooq, O., Luongo, O., & Ratra, B. 2014, *PhRvD*, 90, 044016 [arXiv:1403.1421]
- Chen, G., Gott, J. R., & Ratra, B. 2003, *PASP*, 115, 1269 [arXiv:astro-ph/0308099]
- Chen, G., & Ratra, B. 2011a, *PASP*, 123, 1127 [arXiv:1105.5206]
- Chen, Y., Kumar, S., & Ratra, B. 2017, *ApJ*, 835, 86 [arXiv:1606.07316]
- Chen, Y., & Ratra, B. 2011b, *Phys. Lett. B*, 703, 406 [arXiv:1106.4294]
- Clarkson, C., Bassett, B., & Lu, T. H.-C. 2008, *PhRvL*, 101, 011201 [arXiv:0712.3457]
- Clarkson, C., Cortès, M., & Bassett, B. 2007, *JCAP*, 0708, 011 [arXiv:astro-ph/0702670]
- Delubac, T., Bautista, J. E., Busca, N. G., et al. 2015, *A&A*, 574, A59 [arXiv:1404.1801]
- Dhawan, S., Jha, S. W., & Leibundgut, B. 2018, *A&A*, 609, A72 [arXiv:1707.00715]
- Farooq, O., Crandall, S., & Ratra, B. 2013b, *Phys. Lett. B*, 726, 72 [arXiv:1305.1957]
- Farooq, O., Madiyar, F. R., Crandall, S., & Ratra, B. 2017, *ApJ*, 835, 26 [arXiv:1607.03537]
- Farooq, O., Mania, D., & Ratra, B. 2013a, *ApJ*, 764, 138 [arXiv:1211.4253]
- Farooq, O., Mania, D., & Ratra, B. 2015, *Ap&SS*, 357, 11 [arXiv:1308.0834]
- Farooq, O., & Ratra, B. 2013, *ApJ*, 766, L7 [arXiv:1301.5243]
- Fernández Arenas, D., Terlevich, E., Terlevich, R., et al. 2017, arXiv:1710.05951
- Font-Ribera, A., Kirkby, D., Busca, N., et al. 2014, *JCAP*, 1405, 027 [arXiv:1311.1767]
- Foreman-Mackey, D., Hogg, D. W., Lang, D., & Goodman, J. 2013, *PASP*, 125, 306 [arXiv:1202.3665]
- Gott, J. R. 1982, *Nature*, 295, 304
- Gott, J. R., Vogeley, M. S., Podariu, S., & Ratra, B. 2001, *ApJ*, 549, 1 [arXiv:astro-ph/0006103]
- Hawking, S. W. 1984, *Nucl. Phys. B*, 239, 257
- Holsclaw, T., Alam, U., Sansó, B., et al. 2010a, *PhRvD*, 82, 103502 [arXiv:1009.5443]
- Holsclaw, T., Alam, U., Sansó, B., et al. 2010b, *PhRvL*, 105, 241302 [arXiv:1011.3079]
- Holsclaw, T., Alam, U., Sansó, B., et al. 2011, *PhRvD*, 84, 083501 [arXiv:1104.2041]
- Huterer, D., & Shafer, D. L. 2018, *Rept. Prog. Phys.*, 81, 016901 [arXiv:1709.01091]
- Jesus, J. F., Holanda, R. F. L., & Pereira, S. H. 2017, arXiv:1712.01075
- L'Huilier, B., & Shafeloo, A. 2017, *JCAP*, 1701, 015 [arXiv:1606.06832]
- Li, Y.-L., Li, S.-Y., Zhang, T.-J., & Li, T.-P. 2014, *ApJ*, 789, L15 [arXiv:1404.0773]
- Li, Z., Wang, G.-J., Liao, K., & Zhu, Z.-H. 2016, *ApJ*, 833, 240 [arXiv:1611.00359]
- Lin, W., & Ishak, M. 2017, *PhRvD*, 96, 083532 [arXiv:1708.09813]
- Lonappan, A. I., Ruchika, & Sen, A. A. 2017, arXiv:1705.07336
- Luković, V. V., D'Agostino, R., & Vittorio, N. 2016, *A&A*, 595, A109 [arXiv:1607.05677]
- Magana, J., Amante, M. H., Garcia-Aspeitia, M. A., & Motta, V. 2017, arXiv:1706.09848
- Martin, J., 2012, *C. R. Physique*, 13, 566 [arXiv:1205.3365]
- Martins, C. J. A. P. 2017, *Rept. Prog. Phys.*, 80, 126902 [arXiv:1709.02923]
- Maturi, M., & Mignone, C. 2009, *A&A*, 508, 45 [arXiv:0905.1590]
- Mignone, C., & Bartelmann, M. 2008, *A&A*, 481, 295 [arXiv:0711.0370]
- Mitra, S., Choudhury, T. R., & Ratra, B., 2017, arXiv:1712.00018
- Montiel, A., Lazkoz, R., Sendra, I., et al. 2014, *PhRvD*, 89, 043007 [arXiv:1401.4188]
- Moresco, M. 2015, *MNRAS*, 450, L16 [arXiv:1503.01116]
- Moresco, M., Cimatti, A., Jimenez, R., et al. 2012, *JCAP*, 1208, 006 [arXiv:1201.3609]
- Moresco, M., Pozzetti, L., Cimatti, A., et al. 2016, *JCAP*, 1605, 014 [arXiv:1601.01701]
- Mörtsell, E., & Jönsson, J. 2011, arXiv:1102.4485
- Ooba, J., Ratra, B., & Sugiyama, N. 2017a, arXiv:1707.03452
- Ooba, J., Ratra, B., & Sugiyama, N. 2017b, arXiv:1710.03271
- Ooba, J., Ratra, B., & Sugiyama, N. 2017c, arXiv:1712.08617
- Park, C.-G., & Ratra, B. 2018, arXiv:1801.00213
- Peebles, P. J. E. 1984, *ApJ*, 284, 439
- Peebles, P. J. E., & Ratra, B. 1988, *ApJ*, 325, L17
- Planck Collaboration, Ade, P. A. R., Aghanim, N., Arnaud, M., et al. 2016, *A&A*, 594, A13 [arXiv:1502.01589]



- Podariu, S., & Ratra, B. 2001, *ApJ*, 532, 109  
[arXiv:astro-ph/9910527]
- Rana, A., Jain, D., Mahajan, S., & Mukherjee, A. 2017, *JCAP*, 1703, 028 [arXiv:1611.07196]
- Ratra, B. 1985, *PhRvD*, 31, 1931
- Ratra, B. 2017, *PhRvD*, 96, 103534 [arXiv:1707.03439]
- Ratra, B., & Peebles, P. J. E. 1988, *PhRvD*, 37, 3406
- Ratra, B., & Peebles, P. J. E. 1994, *ApJ*, 432, L5
- Ratra, B., & Peebles, P. J. E. 1995, *PhRvD*, 52, 1837
- Ratra, B., & Vogeley, M. 2008, *PASP*, 120, 235  
[arXiv:0706.1565]
- Ratsimbazafy, A. L., Loubser, S. I., Crawford, S. M., et al. 2017, *MNRAS*, 467, 3239 [arXiv:1702.00418]
- Rezaei, M., Malekjani, M., Basilakos, S., et al. 2017, *ApJ*, 843, 65 [arXiv:1706.02537]
- Riess, A. G., Macri, L. M., Hoffmann, S. L., et al. 2016, *ApJ*, 826, 56 [arXiv:1604.01424]
- Rigault, M., Aldering, G., Kowalski, M., et al. 201, *ApJ*, 802, 20 [arXiv:1412.6501]
- Ross, A. J., Samushia, L., Howlett, C., et al. 2015, *MNRAS*, 449, 835 [arXiv:1409.3242]
- Sahni, V., Shafieloo, A., & Starobinsky, A. A. 2008, *PhRvD*, 78, 103502 [arXiv:0807.3548]
- Samushia, L., Chen, G., & Ratra, B. 2007, arXiv:0706.1963
- Samushia, L., & Ratra, B. 2006, *ApJL*, 650, L5  
[arXiv:astro-ph/0607301]
- Sapone, D., Majerotto, E., & Nesseris, S. 2014, *PhRvD*, 90, 023012 [arXiv:1402.2236]
- Seikel, M., Clarkson, C., & Smith, M. 2012a, *JCAP*, 1206, 036 [arXiv:1204.2832]
- Seikel, M., Yahya, S., Maartens, R., & Clarkson, C. 2012b, *PhRvD*, 86, 083001 [arXiv:1205.3431]
- Shafieloo, A., Kim, A. G., & Linder, E. V. 2012, *PhRvD*, 85, 123530 [arXiv:1204.2272]
- Semiz, İ., & Çamlıbel, A. K. 2015, *JCAP*, 1512, 038  
[arXiv:1505.04043]
- Sievers, J. L., Hlozek, R. A., Nolta, M. R., et al. 2013, *JCAP*, 1310, 060 [arXiv:1301.0824]
- Simon, J., Verde, L., & Jimenez, R. 2005, *PhRvD*, 71, 123001 [arXiv:astro-ph/0412269]
- Stern, D., Jimenez, R., Verde, L., et al. 2010, *JCAP*, 1002, 008 [arXiv:0907.3152]
- Takada, M., & Doré O. 2015, *PhRvD*, 92, 123518  
[arXiv:1508.02469]
- Tripathi, A., Sangwan, A., & Jassal, H. K. 2017, *JCAP*, 1706, 012 [arXiv:1611.01899]
- Vitenti, S. D. P., & Penna-Lima, M. 2015, *JCAP*, 1509, 045 [arXiv:1505.01883]
- Wang, D., & Meng, X. 2017, *Sci. China Phys. Mech. Astron.*, 60, 110411 [arXiv:1610.01202]
- Wang, G.-J., Wei, J.-J., Li, Z.-X., et al. 2017a, *ApJ*, 847, 45  
[arXiv:1709.07258]
- Wang, Y., Xu, L., & Zhao, G.-B. 2017b, *ApJ*, 849, 84  
[arXiv:1706.09149]
- Wei, J.-J., & Wu, X.-F. 2017, *ApJ*, 838, 160  
[arXiv:1611.00904]
- Xia, J.-Q., Yu, H., Wang, G.-J., et al. 2017, *ApJ*, 834, 75  
[arXiv:1611.04731]
- Yahya, S., Seikel, M., Clarkson, C., et al. 2014, *PhRvD*, 89, 023503 [arXiv:1308.4099]
- Yu, H., & Wang, F. Y. 2016, *ApJ*, 828, 85  
[arXiv:1605.02483]
- Yu, H., & Wang, F. Y. 2017, *A&A*, 606, A3  
[arXiv:1708.06905]
- Zhang, B. R., Childress, M. J., Davis, T. M., et al. 2017, *MNRAS*, 471, 2254 [arXiv:1706.07573]
- Zhang, C., Zhang, H., Yuan, S., et al. 2014, *Res. Astron. Astrophys.*, 14, 1221 [arXiv:1207.4541]